ACS APPLIED MATERIALS & INTERFACES

Research Article

www.acsami.org

Core–Corona Functionalization of Diblock Copolymer Micelles by Heterogeneous Metal Nanoparticles for Dual Modality in Chemical Reactions

Seong Ho Jo,[†] Hyun Woo Kim,[†] Minkyung Song,[‡] Nam Jin Je,[†] Sung-hoon Oh,[§] Byoung-Yong Chang,[§] Jinhwan Yoon,[∥] Joo Hyun Kim,[†] Bonghoon Chung,[⊥] and Seong Il Yoo*[,†]

[†]Department of Polymer Engineering and [‡]The Institute of Cleaner Production and Technology, Pukyong National University, 365 Sinseon-ro, Nam-gu, Busan 608-739, Korea

[§]Department of Chemistry, Pukyong National University, 45 Yongso-ro, Nam-gu, Busan 608-739, Korea

[∥]Department of Chemistry, Dong-A University, Nakdong-Daero 550beon-gil, Saha-gu, Busan 608-739, Korea

[⊥]Products Solution Research Group, Global R&D Center, POSCO, Songdo-dong, Yeonsu-gu, Incheon 406-840, Korea

Supporting Information

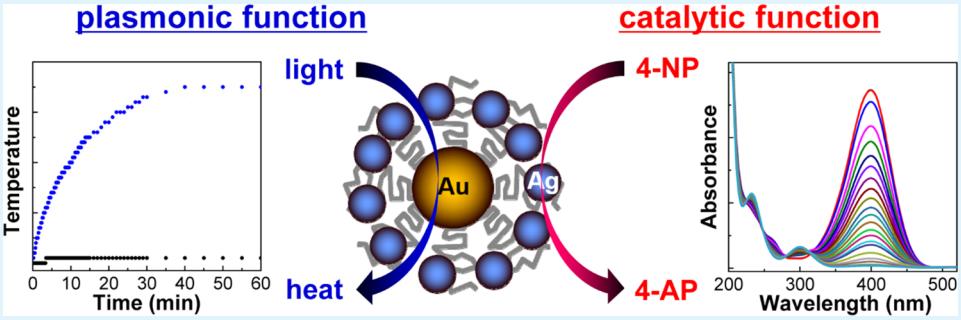

ABSTRACT: Nanoscale assemblies composed of different types of nanoparticles (NPs) can reveal interesting aspects about material properties beyond the functions of individual constituent NPs. This research direction may also represent current challenges in nanoscience toward practical applications. With respect to the assembling method, synthetic or biological nanostructures can be utilized to organize heterogeneous NPs in specific sites via chemical or physical interactions. However, those assembling methods often encounter uncontrollable particle aggregation or phase separation. In this study, we anticipated that the self-segregating properties of block copolymer micelles could be particularly useful for organizing heterogeneous NPs, because the presence of chemically distinct domains such as the core and the corona can facilitate the selective placement of constituent NPs in separate domains. Here, we simultaneously functionalized the core and the corona of micelles by Au NPs and Ag NPs, which exhibited plasmonic and catalytic functions, respectively. Our primary question is whether these plasmonic and catalytic functions can be combined in the assembled structures to engineer the kinetics of a model chemical reaction. To test this hypothesis, the catalytic reduction of 4-nitrophenol was selected to evaluate the collective properties of the micellar assemblies in a chemical reaction.

KEYWORDS: *diblock copolymer, micelle, metal nanoparticle, assembly, surface plasmon, catalyst*

INTRODUCTION

Metal nanoparticles (NPs) have been intensively studied in chemical reactions, as they can catalyze many reactions, including organic synthesis, redox reactions, and the decomposition of pollutants.[1−5] As metal-catalyzed reactions occur for molecules adsorbed on the metal surface, metal NPs having a larger surface-to-volume ratio potentially provide the higher catalytic activity and have a more substantial effect on chemical reactions as compared to bulk metal. In this regard, the structural parameters of metal NPs in terms of size, shape, and crystalline structures have been widely engineered in an attempt to optimize their catalytic performance in a given chemical reaction.[2−5]

In another point of view, metal NPs have stimulated widespread interest in photonics, electronics, and biology because of their localized surface plasmon resonance (LSPR) property.[6−9] LSPR is a collective oscillation of conduction electrons in metal NPs that is resonantly excited by light of a specific frequency. This, in turn, gives rise to a strongly enhanced absorption and scattering of incident light by metal NPs at the resonant frequency, which has a direct relevance to the practical aspects of metal NPs.[6−25] For instance, metal NPs

Received: June 18, 2015
Accepted: August 4, 2015
Published: August 4, 2015

DOI: 10.1021/acsami.5b05408
ACS Appl. Mater. Interfaces 2015, 7, 18778−18785

with a superior scattering property can emit photons having the same frequency with LSPR.[7,9−11] Since the resonantly scattered photons can be easily detected by conventional dark-field microscopy, those NPs hold great promise for biological imaging and are also responsible for enhanced optical signals such as fluorescence in the proximity of the NP surface.[9−12] On the other hand, absorption is a nonradiative process and is correlated with energy dissipation via lattice vibrations or the Joule effect.[7,9,13,14] This results in the generation of heat and an increase in temperature of NPs and the surroundings, which have been utilized for the development of temperature-responsive biological or chemical systems.[7,15−17]

Perceiving that metal NPs can behave as a nanoscale source for catalytic activity, light, and heat, one can raise an interesting question on whether the catalytic and plasmonic functions of metal NPs can be combined so as to modify the kinetics of chemical reactions.[18−20] As a matter of fact, this question is a direct consequence from the knowledge that rate constants (k) of chemical reactions mostly follow the Arrhenius expression, $k = A\exp(-E_a/RT)$, from which the activation energy (E_a) and temperature (T) can be potentially engineered by the aforementioned NP effects. This fundamental question starts to be addressed by recent experimental and theoretical studies, albeit to a limited extent.[18,19,21,24,25] For instance, the combination of heating and catalytic effects of Au NPs has been exploited in several chemical reactions, including the reduction of hexacyanoferrate(III)[24] and Diels−Alder cycloaddition.[25] In those experiments, the temperature of the reaction medium increases upon the excitation of LSPR of Au NPs, which thermally accelerates a given chemical reaction. Simultaneously, the same Au NPs in the reaction medium also serve as a catalyst for reducing the activation energy.

These recent findings clearly highlight innovative aspects of the effects of NPs on chemical reactions; however, the fundamental understanding of these observed NP effects remains elusive in many cases because of the mixed catalytic and plasmonic functions. In particular, there is little clarity on the extent to which plasmonic effects can contribute to the observed catalytic reactions. In this regard, development of a model system that can resolve these mixed NP effects into constituent plasmonic and catalytic functions is necessary to obtain a better insight on NP effects. Although this research direction has mostly fundamental importance, it can also reveal interesting aspects about practical chemical reactions. One of the promising ways to approach this direction can be suggested as the utilization of nano- or mesostructures that can separate plasmonic and catalytic moieties into specific domains in a manner such that the light or heat harvested by the plasmonic function can be utilized by the catalytic sites.

As a new step toward this research direction, we report the nanoscale organization of heterogeneous metal NPs with plasmonic and catalytic functions. Herein, we envisioned that the self-segregating properties of diblock copolymer micelles can be particularly useful for the spatial arrangement of NPs because (1) the presence of chemically distinct domains such as the core and the corona can facilitate the selective placement of different types of metal NPs in separate regions and (2) plasmon hybridization between metal NPs in the core and the corona can be inhibited by their separation in the micellar structure. In fact, these factors allow for an ideal condition for the independent determination of plasmonic and catalytic functions. As a model study, the catalytic reduction of 4-nitrophenol was examined in the presence of micellar NP assemblies to evaluate their collective properties in chemical reactions. Even though the combined effect of the plasmonic and catalytic functions was not observed in the current study, this work still offers a blueprint to engineer NPs at the nanoscale for the development of plasmonic-assisted catalytic systems in future studies.

EXPERIMENTAL SECTION

Polystyrene-*block*-poly(acrylic acid), PS−PAA, diblock copolymer was obtained from ATRP Solution Inc. The degree of polymerization of PS and PAA in the PS−PAA copolymers was 198 and 55, respectively, with a polydispersity index of 1.12. All the other chemicals were purchased from Sigma-Aldrich and were used as received.

Au NPs were synthesized by the citrate reduction of $HAuCl_4{\cdot}3H_2O$. Briefly, an aqueous solution of $HAuCl_4{\cdot}3H_2O$ (1.0 g in 500 mL) was heated until boiling, and 25 mL of sodium citrate solution (0.5 g in 25 mL) was added to the boiling solution. The mixture was further boiled for 15 min with vigorous stirring and then cooled to room temperature. The surfaces of Au NPs were modified by ligand exchange reaction using 2-naphthalenethiol, a hydrophobic ligand. To this end, the as-prepared Au NPs were centrifuged (11,000 rpm, 15 min) two times and then redispersed into *N*,*N*-dimethylformamide (DMF). Subsequently, 2-naphthalenethiol (90 μL, 1.0 wt % in DMF) was added to the purified Au NP solution (9 mL), which was further incubated at 60 °C for 1 h to complete surface modification. In this step, a number of hydrophobic ligands including dodecanethiol can be utilized instead of 2-naphthalenethiol for the same purpose.

PS−PAA micelles containing Au NPs in the core were prepared according to a literature method with slight modification.[26] First, independently prepared DMF solutions of 2-naphthalenethiol-modified Au NPs (4.5 mL) and PS−PAA copolymers (4.5 mL, 0.1 wt % in DMF) were mixed together. Second, deionized water (2 mL) was added to the solution mixture such that the H_2O concentration in the total solution becomes ∼18 vol %. Third, the mixture was heated to 110 °C for 2 h and then slowly cooled to room temperature. Next, the solution was dialyzed against H_2O to remove DMF and residual reagents. In a typical dialysis process, the mixture solution (30 mL) was added to a dialysis membrane having molecular weight cutoff of 3.5 kDa (Spectra/Por7 purchased from Spectrum Laboratories Inc.). After clamping, the dialysis membrane was placed in a large beaker filled with H_2O, which was then gently stirred at room temperature. Deionized water was exchanged for each 12 h at least two times. After dialysis, the solution contained PS−PAA micelles with Au NPs in the core and empty micelles without NPs. Then, the resulting solution was further centrifuged at 11,000 rpm for 30 min to precipitate only the Au NP-containing micelles at the bottom of the centrifugation tube. Finally, the empty micelles were carefully removed along with the supernatant. This removal process was repeated by twice. The final concentration of PS−PAA micelles with the Au NPs was adjusted with H_2O until the absorbance of the solution at 535 nm became 1.0 when monitored by UV−Vis spectroscopy with a cuvette having a path length of 1.0 cm. To further synthesize Ag NPs in the PAA corona, an aliquot of an aqueous $AgNO_3$ solution (30 μL, 0.01 M) was added to 2 mL of the solution of Au NP-containing micelles in a quartz cuvette. Then, the mixture was exposed to UV light (∼254 nm) using a conventional UV lamp (6 W, Vilber Lourmat) in a dark container for different time periods.

The catalytic function was evaluated by the reduction of 4-nitrophenol using excess $NaBH_4$ in the presence and absence of micellar NP assemblies (hereafter denoted as Au@PS−PAA@Ag). For the reaction, the concentration of the as-prepared Au@PS−PAA@Ag assemblies was diluted by 10 times to slow down the reduction rate (see main text for further discussion). Under typical reaction conditions, first, 0.2 mL of an aqueous 4-nitrophenol solution (1.4 mM) was added to H_2O (1.4 mL) in a quartz cuvette. Second, a freshly prepared $NaBH_4$ solution (0.2 mL, 0.42 M) was added to the solution, at which stage the color of the reaction mixture immediately changed from light yellow to dark yellow. Subsequently, 0.2 mL of Au@PS−PAA@Ag assemblies was added to the reaction mixture to

DOI: 10.1021/acsami.5b05408
ACS Appl. Mater. Interfaces 2015, 7, 18778−18785

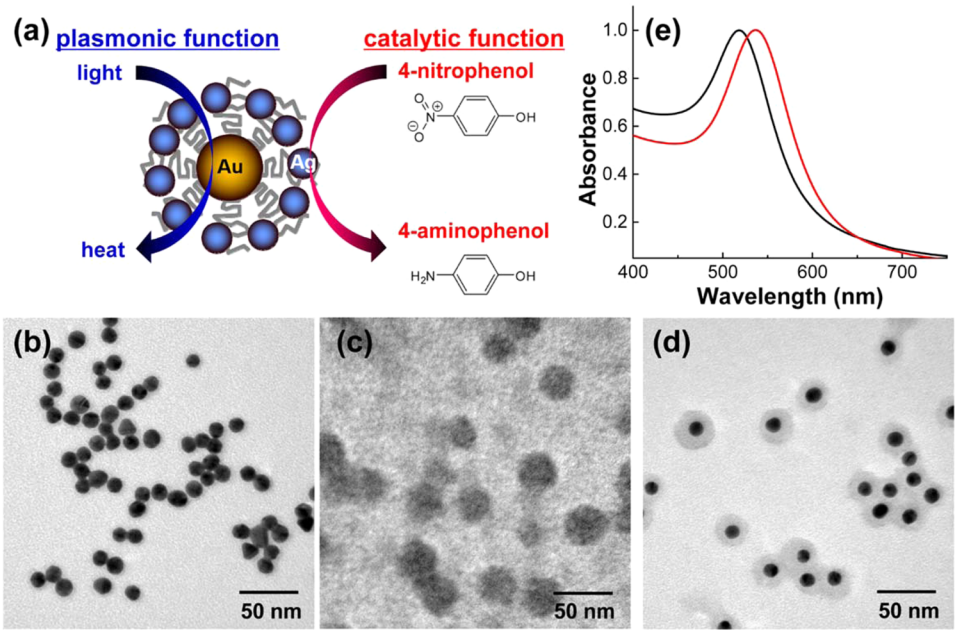

Figure 1. (a) Schematic of heterogeneous NP assemblies. (b–d) TEM images of (b) pure Au NPs, (c) empty PS–PAA micelles, and (d) PS–PAA micelles with Au NP in the core. (e) UV–Vis spectra of pure Au NPs (black) and PS–PAA micelles with the Au NP in the core (red).

initiate the catalytic reaction. To evaluate the plasmonic effect, the reaction mixture in a quartz cuvette was exposed to light-emitting diodes (LEDs, Mightex) having a wavelength of 530 nm. For this purpose, LED light was passed through a focusing lens having a focal length of 30 cm, at which the reaction cuvette was placed. The power of focused LED light was about 16.5 mW/cm^2.

UV–Vis absorbance data were recorded on a JASCO V-670 spectrophotometer. Dynamic light scattering (DLS) and zeta-potential measurements were performed on a Zetasizer Nano ZS-90 (Malvern Instruments). Transmission electron microscopy (TEM) images were recorded on a Hitachi H-7500 instrument operating at 80 kV. High-resolution TEM (HR–TEM) images were recorded on a JEOL JEM-2100F instrument operating at 200 kV. For the TEM image, an aliquot of a solution was dropped on a carbon-coated TEM grid and then dried under ambient conditions.

RESULTS AND DISCUSSION

In a selective solvent, diblock copolymers self-associate into micellar aggregates with insoluble cores and soluble coronas.[26−29] In principle, the presence of chemically distinct domains such as the core and the corona can facilitate the selective placement of functionalities in different regions.[26−29] In this regard, we attempted to functionalize the core and the corona of micelles simultaneously with two different types of metal NPs, i.e., Au NP in the core and Ag NPs in the corona, to provide the plasmonic and catalytic functions in the micellar structures. The schematic of Figure 1a presents the overview of our system that will be discussed throughout this study. For this purpose, PS–PAA copolymers were selected because their aggregation behavior in aqueous solutions has been well studied by the classic work of the Eisenberg group.[29]

In order to functionalize the core of micelles, we first synthesized Au NPs by the citrate-reduction method of $HAuCl_4$. As can be observed in Figure 1b, the synthesized Au NPs are mostly spherical and have negative charges on their surface with a zeta potential value of approximately −35.0 mV, attributed to citrate ions. The Au NP surfaces were modified by ligand exchange reaction using 2-naphthalenethiol, a hydrophobic ligand (see Experimental Section). Then, a DMF solution composed of PS–PAA diblock copolymers, and 2-naphthalenethiol-modified Au NPs was prepared. Since DMF is a good solvent for both PS and PAA blocks, the solution remains homogeneous without any noticeable aggregation at this stage. To initiate micellization, deionized water was added to the DMF solution (H_2O/solution = ∼18 vol %). Subsequently, the solution was heated to 110 °C for 2 h and then slowly cooled to room temperature. In this process, even though H_2O/DMF is a poor solvent for the PS block at room temperature, PS–PAA copolymers are present in their nonaggregated state at 110 °C, which is above the critical micelle temperature.[26] However, during cooling, the PS–PAA copolymers self-associate into spherical micelles consisting of PS cores and PAA coronas. In parallel, 2-naphthalenethiol-modified Au NPs can be encapsulated into the hydrophobic PS cores to prevent unfavorable contact with H_2O/DMF. The resulting solution was further dialyzed against water and centrifuged to remove DMF and residual chemicals. Empty micelles without encapsulated Au NPs, present in the resulting solution because of the excess amount of PS–PAA copolymers, were easily removed by centrifugation.

The encapsulation of Au NPs in the micellar core has been analyzed by several experimental techniques. At first, Figure 1c and 1d show the TEM images of PS–PAA micelles before and after the encapsulation process. By comparing the TEM images, it can be validated that a single Au NP is encapsulated in the center of each micelle; the Au NP can be clearly distinguishable from the micellar structure because of a difference in contrast. From the TEM image, the average diameters of Au NPs and PS–PAA micelles with Au NPs are evaluated as ∼11 nm and ∼35 nm, respectively. Note, Au NPs of this diameter can be considered as a model NP in developing our system because of their uniform size/shape as well as dominant absorption property that will be discussed later. In Figure 1d, PS–PAA copolymers form a uniform shell surrounding the Au NP with a shell thickness of ∼12 nm. Apparently, it is expected that the number of NPs in the micellar core could have a statistical distribution. However, in our experiment, the entire PS–PAA

DOI: 10.1021/acsami.5b05408
ACS Appl. Mater. Interfaces 2015, 7, 18778−18785

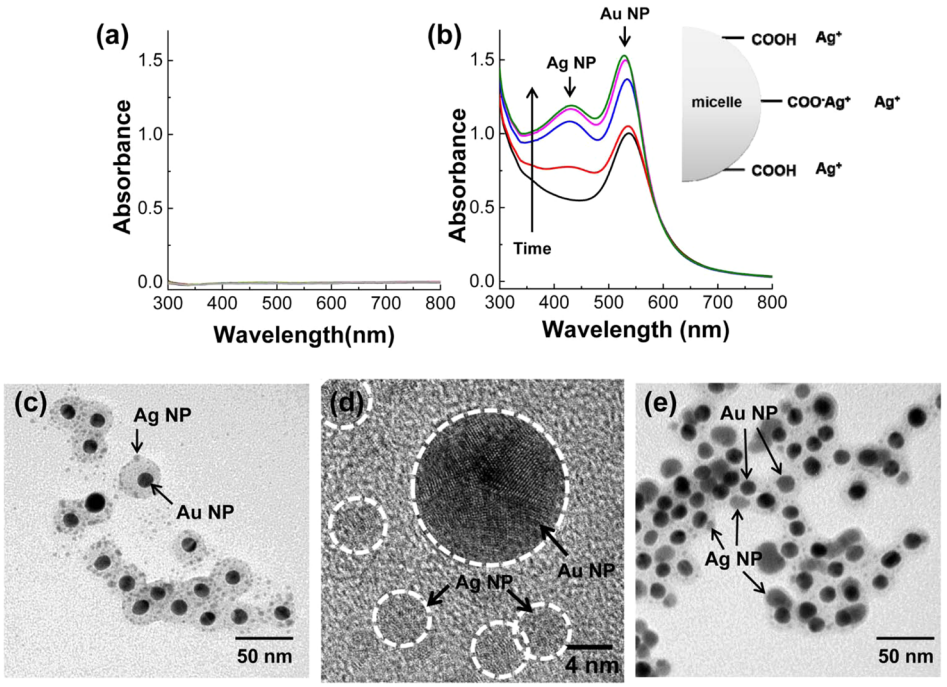

Figure 2. (a, b) Time-dependent UV−Vis spectra from an aqueous $AgNO_3$ solution upon UV irradiation in the absence (a) and presence of (b) Au@PS−PAA micelles. Each color represents different reaction times: black (0 h), red (3 h), blue (6 h), pink (9 h), and green (12 h). (c, d) TEM and HR−TEM images of Au@PS−PAA@Ag micelles after 3 h of reaction. (e) TEM image of Au@PS−PAA@Ag micelles after 12 h of reaction.

micelles contain a single NP in the core, with negligible exception (Supporting Information Figure S1). The rationale behind the single NP encapsulation had been previously discussed by the Taton group.[30] In general, small Au NPs (diameter ≪10 nm) act as solute to dissolve into micelles with multiple NP encapsulation. However, large Au NPs (diameter >10 nm) can work as surface template, onto which polymer chains can be adsorbed.[30] The insertion of the Au NP in the micellar core can be further confirmed by a change in the extinction spectrum. In Figure 1e, the maximum peak in the extinction spectrum of Au NPs shifted from 518 to 535 nm by the encapsulation. Since the extinction position is proportional to the refractive index of the surrounding medium, the red-shifted spectrum further supports the encapsulation of the Au NP in the PS core of micelles.

As a counterpart to the Au NP in the core, Ag NPs were synthesized in the PAA corona of micelles. For this purpose, an aqueous $AgNO_3$ solution was added to the micellar solution to coordinate the carboxylate anions in the PAA block with Ag^+ ions. However, Ag^+ ions are present not only in the PAA block but also in the solvent phase because −COOH is a weak acid. Therefore, in order to synthesize Ag NPs in the corona of micelles, a selective condition has to be employed such that only the immobilized Ag^+ ions can be reduced while preventing the reduction of Ag^+ in the solvent phase. In this circumstance, we employed a photoreduction method by exposing the micellar solution to UV light having a wavelength of 254 nm.[31−33] Here, carboxylate anions in the PAA block can be photoexcited by UV irradiation to assist in the reduction of the immobilized Ag^+ ions.[31−33] However, when an aqueous $AgNO_3$ solution without PS−PAA micelles was employed, UV irradiation alone could not reduce Ag^+ ions, as confirmed by the unchanged UV−Vis spectra from the solution (Figure 2a). On the other hand, reducing Ag^+ ions by chemical reagents such as $NaBH_4$, NH_2OH, and ascorbic acid, other than the photoreduction, resulted in the uncontrolled formation of Ag NPs in the solvent phase, leading to agglomeration and precipitation at the bottom of the solution (data not shown).

In order to monitor the growth of Ag NPs, UV−Vis spectra from the solution were collected at different periods of UV exposure. A typical synthesis went through a continuous increase in the intensities at 430 and 535 nm. As shown in Figure 2b, a new extinction peak of Ag NPs appears at ∼430 nm, which gradually increases with reaction time; in addition, the extinction of the Au NP in the core is clearly discernible at ∼535 nm. It would be worthwhile to note that the absorbance of Ag NPs has a tail on the longer wavelength side, which overlaps with the absorbance of Au NPs. Hence, the growth of Ag NPs entails the gradual increase in both Ag and Au peaks in the UV−vis spectrum. UV exposure time was slightly different for each synthesis; however, the absorbance values typically saturated after 12 h (Supporting Information Figure S2). Since the saturated intensity implies the complete reaction of Ag^+, we selected this condition as the maximum time. For a more quantitative analysis, the atomic concentrations of [Ag] in Au@PS−PAA@Ag assemblies after different photoreduction times were determined by a modified stripping voltammetry, the values of which were evaluated as 0.02 mM (for 3 h), 0.05 mM (for 6 h), and 0.15 mM (for 12 h), respectively (Supporting Information Figure S3). Note, the initial concentration of [Ag^+] was 0.15 mM; hence, this result further supports the complete consumption of Ag^+ ions after 12 h of reaction. In addition, the peak positions of Ag NPs and Au NPs remain nearly unchanged during the reactions. This observation strongly indicates that the two heterogeneous NPs in the core and the corona do not interact because an NP−NP interaction, i.e., plasmon hybridization, is easily detected by a noticeable spectral shift in the extinction.[6,7,34,35] It also turns out that those NP assemblies are quite stable and the plasmonic bands are greatly maintained without noticeable changes in the intensity and position up to 3

DOI: 10.1021/acsami.5b05408
ACS Appl. Mater. Interfaces 2015, 7, 18778−18785

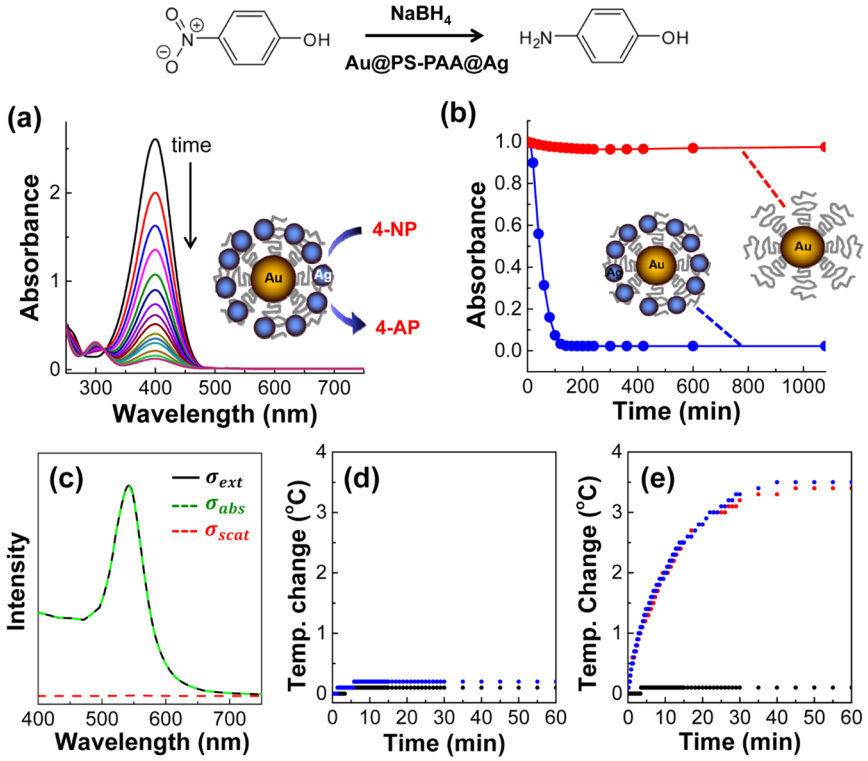

Figure 3. (a) Time-dependent UV−Vis spectra after the addition of Au@PS−PAA@Ag assemblies. (b) Time-dependent absorbance values at 400 nm after the addition of Au@PS−PAA@Ag micelles (blue line) and Au@PS−PAA micelles (red line). The absorbance was normalized by the absorbance value just after the addition of the micellar assembly. (c) Calculated extinction (black solid), absorption (green dotted), and scattering (red dotted) cross sections of Au NPs obtained by the open-source Mieplot v4400 program. The diameter of the Au NPs (11 nm) and the refractive index of the surrounding medium (1.59 for PS) were specified for the calculation. (d, e) Temperature profiles with pure water (black dotted), Au@PS−PAA (red dotted), and Au@PS−PAA@Ag assemblies (blue dotted) upon LED illumination at different concentrations. The mass concentrations of Au@PS−PAA@Ag assemblies are approximately 0.6 wt % (d) and 6.0 wt % (e).

weeks of storage (Supporting Information Figure S4). Based on this result, we can treat those assembled NPs independently for evaluating plasmonic and catalytic functions, the discussion of which will follow.

The formation of a heterogeneous NP assembly in the PS−PAA micelle was further confirmed by TEM analysis (Figure 2). For instance, when the reaction mixture was exposed to UV light for 3 h (corresponding to the red line in the UV−Vis spectrum), small-sized Ag NPs having an average diameter of ∼4 nm were synthesized in Figure 2c. The synthesized NPs are mostly positioned at the peripheral region of the micelles, and this observation further supports the selective synthesis of Ag NPs in the PAA block. At the same time, a single Au NP (average diameter of ∼11 nm) is still placed in the center of the micelles, but is separated from the Ag NPs in the assembled structures. Chemical analysis with energy-dispersive X-ray (EDX) spectra further verified the location of Au and Ag NPs in the assembled structure (Supporting Information Figure S5). The fine partitioning of Au NPs and Ag NPs in the micellar structure can also be confirmed by the HR−TEM image (Figure 2d), in which each NP with lattice structure is marked by dashed circles. We considered that the unchanged extinction peaks in Figure 2b can be attributed to this separation of the Au NP and Ag NPs in the micellar structures.[34,35] When the reaction time was increased to 12 h (corresponding to the green line in the UV−Vis spectrum), the size of the Ag NPs in the periphery substantially increased (Figure 2e), presumably because of the continuous consumption of the unreacted Ag^+ ions in the solvent phase. It appears that Ag NPs mostly get larger on the PAA corona but do not grow toward the PS core when the TEM image is analyzed in combination with the chemical information and UV−vis spectra. At first, the diffusion of Ag^+ ions though the hydrophobic PS core would not be allowed. This implies that Ag NPs mostly get larger on the corona region. Second, if Ag NPs were allowed to grow toward the core, the distance between Au and Ag NPs has to get closer, which will eventually induce a Au−Ag coupling effect. As mentioned before, this coupling effect can be detected by a noticeable shift in the extinction spectrum.[6,7,34,35] However, in our experiments, any meaningful spectral change was not observed in the UV−vis spectra (Figure 2b). Therefore, it could be regarded that the heterogeneous NP assemblies with different reaction time share a common structural feature in terms of the location of the Au NP in the core and partitioning of the Au NP and Ag NPs in a separate location. From this information, the heterogeneous NP assemblies with micellar structure in Figure 2 will be briefly denoted as Au@PS−PAA@Ag hereafter. This kind of heterogeneous NP assemblies can be comparable to those previously found in colloidal science, such as core−satellite assembly[36] or nanomatryoshkas.[15] However, the micellar approach is much more simple and does not require numerous assembling steps. It would also be worthwhile to note that the distance between Au and Ag NPs in the assembled structure can be controlled by employing different-sized PS−PAA micelles (Supporting Information Figure S6).

With the structural characteristics, we focused on the catalytic functions of heterogeneous NP assemblies. In

DOI: 10.1021/acsami.5b05408
ACS Appl. Mater. Interfaces 2015, 7, 18778−18785

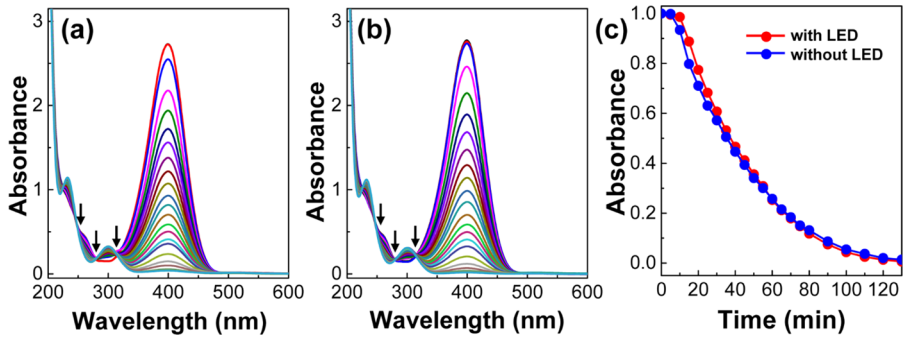

Figure 4. (a, b) Time-dependent UV−Vis spectra in the absence (a) and presence (b) of LED illumination. (c) Time-dependent absorbance at 400 nm in the absence (blue line) and presence (red line) of LED illumination. The absorbance was normalized by the value before the addition of micellar assembly.

particular, the reduction of 4-nitrophenol (4-NP) to 4-aminophenol (4-AP) with excess of $NaBH_4$ was selected as a model reaction because it can be easily monitored by UV−Vis spectroscopy.[37−40] Initially, an aqueous 4-nitrophenol solution typically exhibits a light yellow color with a strong absorbance peak at 317 nm. On adding excess $NaBH_4$, the pH of the solution increases, which results in the conversion of 4-nitrophenol to 4-nitrophenolate ions. This chemical change is accompanied by a red-shift in the absorption maximum from 317 nm (for 4-nitrophenol) to 400 nm (for 4-nitrophenolate ion) with a noticeable change in the solution color to dark yellow. (Supporting Information Figure S7a). Now, it is worth knowing that the reduction of 4-nitrophenol by $NaBH_4$ is thermodynamically favorable from a comparison of the standard reduction potentials of 4-nitrophenol/4-aminophenol = −0.76 V and H_3BO_3/BH_4^- = −1.33 V, respectively.[37,39] However, this reaction is kinetically restricted by the high activation energy and only occurs in the presence of catalyst.[37−40] Owing to these features, the reduction of 4-nitrophenol becomes one of the model reactions for evaluating the catalytic properties of many metal NP systems.

In our experiments, the direct reduction of 4-nitrophenol by $NaBH_4$ did not occur for several days, as confirmed from the unchanged UV−Vis spectra of 4-nitrophenolate (Supporting Information Figure S7). However, as Au@PS−PAA@Ag assemblies were added to the reaction medium, the absorbance at 400 nm started to decrease with reaction time (see Figure 3a), indicative of the catalytic reduction of 4-nitrophenol. Concomitantly, a new absorbance peak appeared at 300 nm and then gradually increased at the same time scale, which can be attributed to the formation of 4-aminophenol.[37−40] It has been reported that the reduction rate of 4-nitrophenol is proportional to the total surface area of metal NPs.[40,41] Therefore, one can reasonably anticipate that smaller NPs would exhibit a higher catalytic activity because of their larger surface-to-volume ratio. In our experiments, when Au@PS−PAA@Ag micelles with small-sized Ag NPs having a diameter of 4 nm (Figure 2c) were employed, reduction was rapid, such that it could not be reasonably monitored by a conventional UV−Vis spectroscope. In this regard, we employed Au@PS−PAA@Ag assemblies under saturated growth conditions (12 h of UV irradiation) in Figure 2e to slow down the rate. Also note the absorbance change at 400 nm is significantly stronger than that at 300 nm (Figure 3a). Hence, we extracted the time-dependent absorbance values at 400 nm from the UV−Vis spectra to closely monitor reaction kinetics (blue color in Figure 3b). For comparison purposes, the catalytic activity of PS−PAA micelles with only Au NP in the core (denoted as Au@PS−PAA hereafter) was also tested, the result of which is depicted in red. From the comparison, it is obvious that the reduction only occurred for Au@PS−PAA@Ag assemblies having Ag NPs in the corona but was practically restricted for Au@PS−PAA assemblies. The restricted catalytic activity of Au@PS−PAA micelles can be attributed to the unfavorable diffusion of 4-nitrophenolate ions to the Au NP through the hydrophobic PS core, as pure Au NPs without a micellar structure efficiently catalyzed the same reaction (Supporting Information Figure S8).

Convinced of the catalytic function of Ag NPs, we turned our attention to the plasmonic function of Au NP in the Au@PS−PAA@Ag assemblies. According to the Mie theory, we first calculated the extinction spectra of the Au NP in the micellar core with constituent absorption and scattering cross sections.[42] As shown in Figure 3c, the Au NP having an average diameter of 11 nm essentially shows an absorption cross section (σ_{abs}) with negligible scattering (σ_{scat}) in its extinction spectrum (σ_{ext}). Note, absorption is a nonradiative process and is closely interconnected with energy dissipation into heat.[7,9,13,14] It has also been reported that the temperature increase around metal NPs can be expressed by $\Delta T \sim \sigma_{abs} I/R$, where σ_{abs} is the absorption cross section, I is the intensity of illuminating light, and R is the radius of the metal NPs.[13,14,18] Therefore, we anticipated that those Au NPs in the micellar core having a superior absorption cross section can efficiently convert the absorbed light into localized heat to increase the temperature of the reaction medium. In this context, we exposed the reaction mixture containing Au@PS−PAA@Ag assemblies to LED light in an attempt to measure the temperature change in the solution. The wavelength of the LED light was chosen as 530 nm to selectively excite LSPR of Au NPs. However, we could not measure any appreciable temperature change in the reaction medium (blue color in Figure 3d), which is a stark contrast to the aforementioned consideration. The temperature change was as marginal as ∼0.2 °C: this value is nearly identical to that observed from pure water in Figure 3d (black).

However, the overall heating effect is the sum of the heating of individual Au NPs; hence, the temperature change of the solution is proportional to the Au NP concentration.[13,14,18] In our experiments, we reduced the concentration of the Au@PS−PAA@Ag assemblies to as low as possible. Typically, the as-prepared Au@PS−PAA@Ag assemblies were 10 times diluted for the catalytic reaction. This dilution was necessary to slow down the rate of reactions; otherwise, the catalytic reduction was too fast to be monitored on a reasonable time scale. In this

DOI: 10.1021/acsami.5b05408
ACS Appl. Mater. Interfaces 2015, 7, 18778−18785

regard, we assumed that the local heat generated by the Au NP could be dissipated into the solvent phase without increasing the bulk temperature. To verify this assumption, we repeated the experiments without diluting the Au@PS−PAA@Ag assemblies. Under this condition, a temperature increase of ∼3.5 °C was clearly detected upon LED illumination (Figure 3e). Therefore, it is quite reasonable to consider that a single Au NP emits heat to elevate the local temperature around the Au NP, even though the temperature change in the actual mixture could not be detected in Figure 3d. Also note the temperature profiles from Au@PS−PAA (red dotted) and Au@PS−PAA@Ag (blue dotted) assemblies are basically the same as each other in Figure 3e, which further verifies the independent plasmonic function of Au NPs in Au@PS−PAA@Ag assemblies.

Having verified the independent properties of Ag NPs and Au NPs in Figure 3, we tested their collective effects on a model chemical reaction. To this end, the reduction of 4-nitrophenol was performed again in the absence (Figure 4a) and presence (Figure 4b) of LED light. Irrespective of LED illumination, a rapid decrease in the absorbance at 400 nm and a concomitant increase at 300 nm are observed. This gives clear evidence of the catalytic effects of the Au@PS−PAA@Ag assemblies in both cases. In parallel, isosbestic points at 248, 280, and 315 nm (denoted by arrows) commonly appeared in Figures 4a and 4b, which further indicates that no secondary reactions occur upon LED illumination. To better examine the influence of LED light and therefore corresponding collective properties, time-dependent absorbance at 400 nm was compared in Figure 4c. Noticeably, the reduction kinetics, in the absence (blue color in Figure 4c) and presence (red color) of LED light, are nearly identical. By using the pseudo-first-order approximation, the rate constant was determined as 0.026 min^{-1} and 0.028 min^{-1} for the reactions in the absence and presence of LED light, respectively (see further discussion in Supporting Information Figure S9), and these two values are basically the same.

This observation is markedly different from the one that we anticipated because the Au@PS−PAA@Ag assemblies are expected to control the reaction rate by simultaneously modifying activation energy (by catalytic effect) and temperature (by plasmonic effect). In this context, the negligible contribution of the plasmonic effect reflects that the overall rate of reaction is mainly governed by the catalytic effect. In fact, as far as our understanding is concerned, the difficulty here in observing the combined plasmonic and catalytic functions could be strongly interconnected with the time scale of the reaction. For instance, in order to enhance the plasmonic effect, the concentration of Au@PS−PAA@Ag assemblies has to be further increased for a noticeable temperature rise (i.e., Figure 3e). However, an increase in the concentration also significantly accelerated the reaction rate so that it could not be monitored by conventional UV−vis spectroscopy.

Nevertheless, this result still offers a blueprint for nanoscale engineering for future development of plasmonic-assisted catalytic systems as follows. Considering that the reaction kinetics mostly follow the Arrhenius law of $k = A\exp(-E_a/RT)$, the influence of LED illumination on rate constant (k) can be expressed as $k/k^0 = \exp[E_a/R(1/T^0 - 1/T)]$, where T^0 and T (or k^0 and k) are the local temperatures around the Ag NPs (or rate constants) in the absence and presence of LED illumination, respectively. Here we assumed that activation energy (E_a) and the pre-exponential factor (A) are the same irrespective of LED illumination because the catalytic function is solely determined by Ag NPs in the corona. Since the reduction kinetics remained unchanged upon LED illumination, the k/k^0 ratio can be set as 1.0. Therefore, the value in the parentheses of the exponential function approaches zero in the current system. This alternatively indicates that, in order to combine the catalytic and plasmonic functions, one has to employ a chemical system with the higher activation energy and/or increase the plasmonic effect in a manner such that the k/k^0 ratio becomes greater than 1.0. As the catalytic and plasmonic functions are strongly dependent on the structural parameters of metal NPs, the systematic tuning of the Au@PS−PAA@Ag assemblies by a suitable selection of the model reactions can support future development.

CONCLUSIONS

In this study, we developed a simple and versatile method to organize heterogeneous NPs in a framework of diblock copolymer micelles. The self-segregating properties of PS−PAA micelles enabled the nanoscale arrangement of heterogeneous NPs, in which Au NP in the core is surrounded by Ag NPs in the corona. The resulting Au@PS−PAA@Ag assemblies exhibited both plasmonic and catalytic functions, which have been further applied to control the kinetics of a model chemical reaction. As a relevant future direction, we are pursuing the fine control of the structural parameters of the Au@PS−PAA@Ag assemblies in terms of the size/shape of metal NPs as well as the size of micelles to further develop plasmonic-assisted catalytic systems. In particular, efficient energy transduction could be realized by delivering the heat or light harvested by plasmonic NPs in the core to the catalytic NPs in the corona. It would also be interesting to anticipate that the actual function of each NP would be determined by its location in the assembled structures. For instance, if Ag@PS−PAA@Au assemblies having an opposite NP configuration could be prepared, the role of each NP will be switched with each other. Indeed, a number of interesting opportunities are present in the micellar NP assemblies.

ASSOCIATED CONTENT

Supporting Information

The Supporting Information is available free of charge on the ACS Publications website at DOI: 10.1021/acsami.5b05408.

Additional TEM images, EDX spectra, UV−vis spectra, and stripping voltammograms with further discussions (PDF)

AUTHOR INFORMATION

Corresponding Author

*Tel: +82-51-629-6456; Fax: +82-51-629-6429; E-mail: siyoo@pknu.ac.kr.

Notes

The authors declare no competing financial interest.

ACKNOWLEDGMENTS

This research was supported by the Basic Science Research Program through the National Research Foundation of Korea (NRF), funded by the Ministry of Science, ICT & Future Planning (NRF-2012R1A1A1001453), and Basic Science Research Program through the National Research Foundation of Korea (NRF), funded by the Ministry of Education (NRF-2014R1A1A2056167).

DOI: 10.1021/acsami.5b05408
ACS Appl. Mater. Interfaces 2015, 7, 18778−18785

REFERENCES

(1) Bell, A. T. The Impact of Nanoscience on Heterogeneous Catalysis. *Science* **2003**, *299*, 1688−1691.
(2) Zaera, F. New Challenges in Heterogeneous Catalysis for the 21st Century. *Catal. Lett.* **2012**, *142*, 501−506.
(3) Somorjai, G. A.; Park, J. Y. Molecular Factors of Catalytic Selectivity. *Angew. Chem., Int. Ed.* **2008**, *47*, 9212−9228.
(4) Lee, I.; Morales, R.; Albiter, M. A.; Zaera, F. Synthesis of Heterogeneous Catalysts with Well-Shaped Platinum Particles To Control Reaction Selectivity. *Proc. Natl. Acad. Sci. U. S. A.* **2008**, *105*, 15241−15246.
(5) Xiong, Y.; Wiley, B. J.; Xia, Y. Nanocrystals with Unconventional Shapes—A Class of Promising Catalysts. *Angew. Chem., Int. Ed.* **2007**, *46*, 7157−7159.
(6) Halas, N. J.; Lal, S.; Chang, W.-S.; Link, S.; Nordlander, P. Plasmons in Strongly Coupled Metallic Nanostructures. *Chem. Rev.* **2011**, *111*, 3913−3961.
(7) Rycenga, M.; Cobley, C. M.; Zeng, J.; Li, W.; Moran, C. H.; Zhang, Q.; Qin, D.; Xia, Y. Controlling the Synthesis and Assembly of Silver Nanostructures for Plasmonic Applications. *Chem. Rev.* **2011**, *111*, 3669−3712.
(8) Atwater, H. A.; Polman, A. Plasmonics for Improved Photovoltaic Devices. *Nat. Mater.* **2010**, *9*, 205−213.
(9) Jain, P. K.; El-Sayed, I. H.; El-Sayed, M. A. Au Nanoparticles Target Cancer. *Nano Today* **2007**, *2*, 18−29.
(10) Raschke, G.; Kowarik, S.; Franzl, T.; Sönnichsen, C.; Klar, T. A.; Feldmann, J. Biomolecular Recognition Based on Single Gold Nanoparticle Light Scattering. *Nano Lett.* **2003**, *3*, 935−938.
(11) McFarland, A. D.; Van Duyne, R. P. Single Silver Nanoparticles as Real-Time Optical Sensors with Zeptomole Sensitivity. *Nano Lett.* **2003**, *3*, 1057−1062.
(12) Lakowicz, J. R.; Ray, K.; Chowdhury, M.; Szmacinski, H.; Fu, Y.; Zhang, J.; Nowaczyk, K. Plasmon-Controlled Fluorescence: A New Paradigm in Fluorescence Spectroscopy. *Analyst* **2008**, *133*, 1308−1346.
(13) Baffou, G.; Quidant, R.; de Abajo, F. J. G. Nanoscale Control of Optical Heating in Complex Plasmonic Systems. *ACS Nano* **2010**, *4*, 709−716.
(14) Govorov, A. O.; Richardson, H. H. Generating Heat with Metal Nanoparticles. *Nano Today* **2007**, *2*, 30−38.
(15) Ayala-Orozco, C.; Urban, C.; Knight, M. W.; Uran, S. A.; Neumann, O.; Bishnoi, S. W.; Mukherjee, S.; Goodman, A. M.; Charron, H.; Mitchell, T.; Shea, M.; Roy, R.; Nanda, S.; Schiff, R.; Halas, N. J.; Joshi, A. Au Nanomatryoshkas as Efficient Near-Infrared Photothermal Transducers for Cancer Treatment: Benchmarking against Nanoshells. *ACS Nano* **2014**, *8*, 6372−6381.
(16) He, J.; Huang, X.; Li, Y.-C.; Liu, Y.; Babu, T.; Aronova, M. A.; Wang, S.; Lu, Z.; Chen, X.; Nie, Z. Self-Assembly of Amphiphilic Plasmonic Micelle-Like Nanoparticles in Selective Solvents. *J. Am. Chem. Soc.* **2013**, *135*, 7974−7984.
(17) Croissant, J.; Zink, J. I. Nanovalve-Controlled Cargo Release Activated by Plasmonic Heating. *J. Am. Chem. Soc.* **2012**, *134*, 7628−7631.
(18) Baffou, G.; Quidant, R. Nanoplasmonics for Chemistry. *Chem. Soc. Rev.* **2014**, *43*, 3898−3907.
(19) Qiu, J.; Wei, W. D. Surface Plasmon-Mediated Photothermal Chemistry. *J. Phys. Chem. C* **2014**, *118*, 20735−20749.
(20) Kale, M. J.; Avanesian, T.; Christopher, P. Direct Photocatalysis by Plasmonic Nanostructures. *ACS Catal.* **2014**, *4*, 116−128.
(21) Wang, F.; Li, C.; Chen, H.; Jiang, R.; Sun, L.-D.; Li, Q.; Wang, J.; Yu, J. C.; Yan, C.-H. Plasmonic Harvesting of Light Energy for Suzuki Coupling Reactions. *J. Am. Chem. Soc.* **2013**, *135*, 5588−5601.
(22) Hung, W. H.; Aykol, M.; Valley, D.; Hou, W.; Cronin, S. B. Plasmon Resonant Enhancement of Carbon Monoxide Catalysis. *Nano Lett.* **2010**, *10*, 1314−1318.
(23) Chen, X.; Zhu, H.-Y.; Zhao, J.-C.; Zheng, Z.-F.; Gao, X.-P. Visible-Light-Driven Oxidation of Organic Contaminants in Air with Gold Nanoparticle Catalysts on Oxide Supports. *Angew. Chem., Int. Ed.* **2008**, *47*, 5353−5356.
(24) Yen, C.-W.; El-Sayed, M. A. Plasmonic Field Effect on the Hexacyanoferrate (III)-Thiosulfate Electron Transfer Catalytic Reaction on Gold Nanoparticles: Electromagnetic or Thermal? *J. Phys. Chem. C* **2009**, *113*, 19585−19590.
(25) Vázquez-Vázquez, C.; Vaz, B.; Giannini, V.; Pérez-Lorenzo, M.; Alvarez-Puebla, R. A.; Correa-Duarte, M. A. Nanoreactors for Simultaneous Remote Thermal Activation and Optical Monitoring of Chemical Reactions. *J. Am. Chem. Soc.* **2013**, *135*, 13616−13619.
(26) Yang, M.; Chen, T.; Lau, W. S.; Wang, Y.; Tang, Q.; Yang, Y.; Chen, H. Development of Polymer-Encapsulated Metal Nanoparticles as Surface-Enhanced Raman Scattering Probes. *Small* **2009**, *5*, 198−202.
(27) Mai, Y.; Eisenberg, A. Selective Localization of Preformed Nanoparticles in Morphologically Controllable Block Copolymer Aggregates in Solution. *Acc. Chem. Res.* **2012**, *45*, 1657−1666.
(28) Liu, Y.; Wang, X. Recent Advances in Block Copolymer-Assisted Synthesis of Supramolecular Inorganic/Organic Hybrid Colloids. *Polym. Chem.* **2011**, *2*, 2741−2757.
(29) Zhang, L.; Eisenberg, A. Multiple Morphologies and Characteristics of "Crew-Cut" Micelle-like Aggregates of Polystyrene-b-poly(acrylic acid) Diblock Copolymers in Aqueous Solutions. *J. Am. Chem. Soc.* **1996**, *118*, 3168−3181.
(30) Kang, Y.; Taton, T. A. Controlling Shell Thickness in Core−Shell Gold Nanoparticles via Surface-Templated Adsorption of Block Copolymer Surfactants. *Macromolecules* **2005**, *38*, 6115−6121.
(31) Shen, Z.; Duan, H.; Frey, H. Water-Soluble Fluorescent Ag Nanoclusters Obtained from Multiarm Star Poly(acrylic acid) as "Molecular Hydrogel" Templates. *Adv. Mater.* **2007**, *19*, 349−352.
(32) Lu, Y.; Mei, Y.; Schrinner, M.; Ballauff, M.; Möller, M. W.; Breu, J. In Situ Formation of Ag Nanoparticles in Spherical Polyacrylic Acid Brushes by UV Irradiation. *J. Phys. Chem. C* **2007**, *111*, 7676−7681.
(33) Zhang, J.; Xu, S.; Kumacheva, E. Photogeneration of Fluorescent Silver Nanoclusters in Polymer Microgels. *Adv. Mater.* **2005**, *17*, 2336−2340.
(34) Sheikholeslami, S.; Jun, Y.-W.; Jain, P. K.; Alivisatos, A. P. Coupling of Optical Resonances in a Compositionally Asymmetric Plasmonic Nanoparticle Dimer. *Nano Lett.* **2010**, *10*, 2655−2660.
(35) Jain, P. K.; Huang, W.; El-Sayed, M. A. On the Universal Scaling Behavior of the Distance Decay of Plasmon Coupling in Metal Nanoparticle Pairs: A Plasmon Ruler Equation. *Nano Lett.* **2007**, *7*, 2080−2088.
(36) Wang, L.; Xu, L.; Kuang, H.; Xu, C.; Kotov, N. A. Dynamic Nanoparticle Assemblies. *Acc. Chem. Res.* **2012**, *45*, 1916−1926.
(37) Seo, E.; Kim, J.; Hong, Y.; Kim, Y. S.; Lee, D.; Kim, B.-S. Double Hydrophilic Block Copolymer Templated Au Nanoparticles with Enhanced Catalytic Activity toward Nitroarene Reduction. *J. Phys. Chem. C* **2013**, *117*, 11686−11693.
(38) Zeng, J.; Zhang, Q.; Chen, J.; Xia, Y. A Comparison Study of the Catalytic Properties of Au-Based Nanocages, Nanoboxes, and Nanoparticles. *Nano Lett.* **2010**, *10*, 30−35.
(39) Saha, S.; Pal, A.; Kundu, S.; Basu, S.; Pal, T. Photochemical Green Synthesis of Calcium-Alginate-Stabilized Ag and Au Nanoparticles and Their Catalytic Application to 4-Nitrophenol Reduction. *Langmuir* **2010**, *26*, 2885−2893.
(40) Mei, Y.; Lu, Y.; Polzer, F.; Ballauff, M. Catalytic Activity of Palladium Nanoparticles Encapsulated in Spherical Polyelectrolyte Brushes and Core−Shell Microgels. *Chem. Mater.* **2007**, *19*, 1062.
(41) Hervés, P.; Pérez-Lorenzo, M.; Liz-Marzán, L.; Dzubiella, J.; Lu, Y.; Ballauff, M. Catalysis by Metallic Nanoparticles in Aqueous Solution: Model Reactions. *Chem. Soc. Rev.* **2012**, *41*, 5577.
(42) *MiePlot: A computer program for scattering of light from a sphere using Mie theory & the Debye series*; http://www.philiplaven.com/mieplot.htm.

DOI: 10.1021/acsami.5b05408
ACS Appl. Mater. Interfaces 2015, 7, 18778−18785